Fatigue performance and damage characterisation of ultra-thin tow-based discontinuous tape composites

N.B. When citing this work, cite the original published paper.
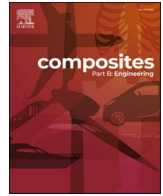
(article starts on next page)

Fatigue performance and damage characterisation of ultra-thin tow-based discontinuous tape composites

Ioannis Katsivalis [a,*], Monica Norrby [b], Florence Moreau [c], Erik Kullgren [d], Soraia Pimenta [e], Dan Zenkert [b], Leif E. Asp [a]

[a] Department of Industrial and Materials Science, Chalmers University of Technology, Sweden
[b] Department of Engineering Mechanics, KTH, Sweden
[c] Oxeon AB, Sweden
[d] Elitkomposit AB, Sweden
[e] Department of Mechanical Engineering, Imperial College London, UK

ARTICLE INFO

ABSTRACT

Tow-based discontinuous composites are an attractive alternative material to conventional continuous composites as they offer in-plane isotropy, enhanced manufacturability allowing to achieve complex 3D shapes with high curvatures and local reinforcement in critical areas, while also maintaining high strength and stiffness, therefore expanding the design space significantly. In addition, the use of ultra-thin tapes and optimised manufacturing methods can increase the mechanical properties even further and change the damage mechanisms. Fatigue, however, could be a limiting design factor, as the fatigue behaviour of these materials has not been fully characterised. This work presents a complete study on the fatigue response of ultra-thin tow-based discontinuous composites: fatigue S–N curves are measured, and the damage and failure mechanisms are characterised utilising optical and scanning electron microscopy. Finally, a critical interpretation of the results is also presented by comparing the performance of ultra-thin tow-based discontinuous composites against other similar fibre reinforced composites and metals. It is shown that the optimised manufacturing methods combined with low tape thickness leads to enhanced quasi-isotropic fatigue performance. In addition, the fatigue limit was raised significantly compared to other discontinuous composites, and the tow-based discontinuous composites outperformed their metal counterparts when the results were normalised with density.

1. Introduction

Carbon Fibre Reinforced Polymers (CFRP) represent one of the most attractive materials for high-end engineering applications such as aircraft design [1] and hydrogen storage [2] due to their high specific strength and stiffness (strength and stiffness to density ratio). Conventional continuous-fibre composites display excellent properties in the fibre direction but are also significantly weaker in the in-plane transverse and out-of-plane directions. Therefore, Quasi-Isotropic (QI) lay-ups, which utilise plies of different orientations, are typically employed in many applications, as they have in-plane isotropic properties and thus simplify the design. However, QI lay-ups also reduce the structural efficiency of composite materials.

A new class of composite materials which have gained significant popularity and represent an attractive alternative to QI laminates are the so-called Tow- (or Tape-) Based Discontinuous Composites (TBDCs) [3]. These materials are manufactured by chopping continuous prepreg tapes (chips) and randomly distributing them, effectively creating a high-performance Sheet Moulding Compound (SMC) material. The random tape distribution generates in-plane isotropy, while the use of very low tape thicknesses (below 50 μm) reduces resin pockets and increases the attainable fibre volume fractions [4]. Using thin tapes also shifts the dominant damage mechanisms, effectively eliminating transverse tape fracture and promoting tape pull-out instead [5]. The latter are related to the in-situ strength effect as described by Camanho et al. [6] and also to the decrease in energy release rate [4], when using thinner tapes. In addition, TBDCs display increased manufacturability and reduced costs and therefore expand the design space significantly. Significant efforts have been made to characterise experimentally [3–5, 7,8] and model numerically [9–11] the quasi-static response of these

---

* Corresponding author.
E-mail address: ioannis.katsivalis@chalmers.se (I. Katsivalis).

materials.

Fatigue is typically a critical design parameter in automotive and aerospace applications especially when metallic components are involved. Metals are very susceptible to fatigue damage as cracks grow due to dislocation migration [12]. However, in CFRP components, due to the amorphous nature of the matrix such dislocation migration cannot be achieved. Therefore, composites are generally considered to display excellent fatigue performance. However, the fatigue performance of composites is also expected to be dependent on the matrix/fibre system, the lay-up sequence, and the ply thickness [13]. In addition, the fatigue crack growth is expected to be governed by the presence of defects and can be accelerated by environmental exposure [14]. During fatigue loading, there are competing damage and failure mechanisms taking place, namely, fibre fracture, matrix cracking, fibre matrix debonding and delamination. The most dominant mechanism depends on the laminate architecture and the applied loading. For instance, Brunbauer and Pinter [15] demonstrated that fatigue loading in the fibre direction leads to fibre breakage and pull-out, while loading in the transverse direction leads to matrix cracking and matrix fibre debonding.

S–N curves are typically employed to describe the fatigue performance of coupons and components. In these curves, *S* represents the applied stress and *N* the applied cycles to failure. Talreja [16] also proposed a framework which is gaining popularity where the strain to failure is plotted against the number of cycles, effectively converting the *S–N* curve to an *ε-N* curve. Talreja [16] also introduced the concept of fatigue life diagram which typically consists of 3 distinct regions for composites under cyclic longitudinal tension. The first region is related to low-cycle fatigue and the strength/strain-to-failure is close to the static values. The second region is the mid-level regime where longer fatigue lives are associated with lower strengths. In this second region, the damage is governed by the progressive propagation of smaller cracks in the fibres or the interfaces, and the number and size of cracks increases until fracture occurs. Eventually, for low values of applied stress/strain, the fatigue life diagram reaches a plateau where no fatigue failure can take place since the stress/strain applied is too low to activate damage. This plateau is the third region, which is also called the fatigue limit region and indicates infinite fatigue life. It is worth noting that there is no clear consensus in the literature whether such a plateau exists for composite materials [17]. Most fatigue studies define the maximum stress level below which the fatigue life of the composite becomes longer than a specified number of cycles to failure (typically 2×10^6 cycles) [14,15,18–20].

While fatigue loading has been studied extensively for continuous fibre composites, there are just a few studies on the fatigue performance of TBDCs and similar materials. Selezneva and Lessard [21] characterised a thermoplastic TBDC type material under various load cases, while they also performed a fatigue study with a stress ratio (ratio between the minimum and maximum stress) of R = 0.1 at four different load levels. The fatigue results of the TBDC material were compared with a QI laminate with similar characteristics, and it was shown that the TBDC material had slightly better fatigue response by displaying a flatter slope in the *S–N* curve. However, it is worth noting that the stress ratio and the testing frequency between the TBDC and the QI laminate were different and thus definite conclusions were difficult to make.

Tang et al. [18] performed a combined experimental and numerical study on the fatigue response of TBDC materials under tension-tension loading. The authors observed large scatter in the obtained *S–N* diagram which was related to the random chip distribution in the specimens. According to the authors, the specimens displayed a heterogeneous stiffness response and failed in areas of low longitudinal modulus. Such observations were also made by other authors during static testing [5,22]. In another study, Tang et al. [23] performed tensile and compressive static tests which were later followed by an extended fatigue testing campaign including tension-tension, compression-compression and tension-compression loading. This study revealed large experimental scatter which was once again attributed to the random

chip orientation. The authors proposed the use of a strength normalisation factor which considers the effect of the fibre orientation and reduces the experimental scatter.

Martulli et al. [24] performed interrupted fatigue testing combined with computed tomography on TBDC specimens and demonstrated that the complicated micro-architecture acts as a crack arresting feature improving the fatigue resistance of TBDC specimens. The experimental results displayed scatter, especially when considering specimens of different orientations. In addition, a theory for the damage evolution during fatigue loading was proposed as follows: at first, intra-tow splitting occurs which is followed by damage propagation through the matrix. Finally, failure occurs because of the reduction of the effective cross section due to multiple propagating cracks.

The authors demonstrated in the past that the static properties of the TBDCs increase significantly when ultra-thin tapes were used [5]. More specifically, the stiffness and strength of the TBDCs utilising 20 μm thick tapes were at least 30 % higher compared to any other value reported in the literature for such materials. It is speculated that the significant increase in the static strength will also lead to an elevated fatigue limit for the same system. However, an experimental study on the fatigue performance of ultra-thin TBDCs under tension-tension fatigue loading is currently lacking.

This paper describes in detail the experimental work related to the fatigue testing, covering specimen manufacturing and preparation, experimental testing, and measurements, and finally damage and fracture characterisation in the macro- and micro-scales. This is the first time that the improved manufacturing methods for the development of randomly oriented discontinuous composites are evaluated under fatigue loading. The presented fatigue results exceed overwhelmingly any other value reported in the literature for discontinuous composites and therefore highlight the real potential of this material in demanding structural applications. The results are also compared with literature values on conventional TBDCs and QI laminates, as well as conventional metals (steel, titanium, and aluminium), highlighting the high-performance potential and versatility of ultra-thin TBDC's even further.

2. Materials and methods

2.1. Plate manufacturing

One plate was manufactured for the fatigue testing of the ultra-thin TBDC material. The plate had dimensions 300 × 300 mm and nominal thickness of 1.2 mm. Fig. 1 shows the plate manufactured pointing out the locations and relative orientation of characteristic specimens. For the manufacturing of the plate, TeXtreme tapes manufactured by Oxeon AB with spread tow technology were used. The PyrofilTM MR70 12 P carbon fibre from Mitsubishi Chemical Carbon Fiber and Composites was used, which has a longitudinal modulus of 325 GPa and strength of 7000 MPa. The tapes were partially impregnated by Oxeon AB to reach a 35%w resin content after curing, and afterwards were cut to size (20 × 40 mm) for the plate manufacturing. The theoretical cured ply thickness of each tape was 21.4 μm (approximate 1/56 of the nominal plate thickness).

An automated process was used to ensure random placement and orientation of every tape. The total number of tapes required was determined by considering the target thickness for each plate. The preforms were slightly pre-consolidated before curing which followed the cycle shown in Fig. 2. The use of pre-impregnated tapes, the automation of the tape placement and the higher moulding pressure allowed to achieve high fibre volume fractions and thus enhanced mechanical performance. Details relating to these manufacturing steps can also be found in Ref. [5]. A band saw with a diamond coated blade was used to cut the specimens from the plate after curing, while specimens were cut in two different orientations as shown in Fig. 1 to validate the quasi-isotropic behaviour. Fig. 3 shows a characteristic cross-section of the TBDC material highlighting the random orientation of the tapes
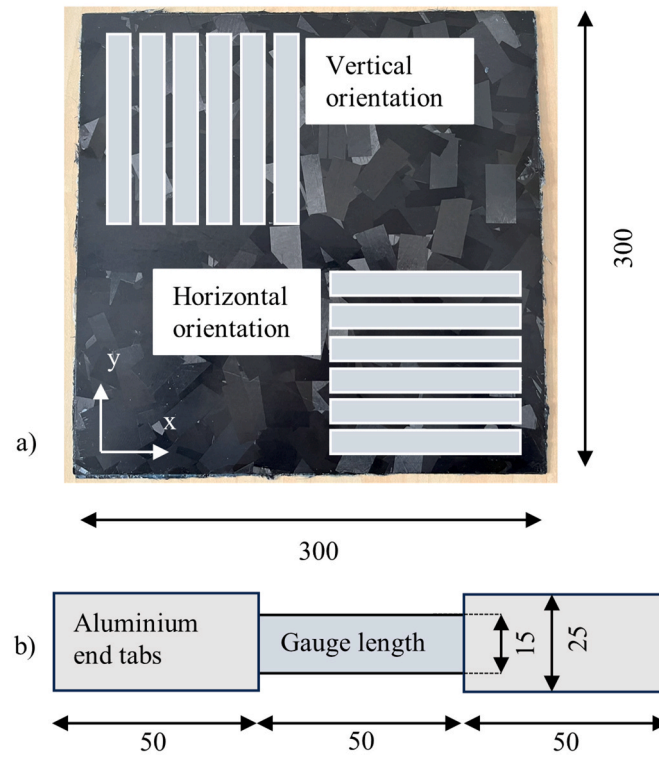
Fig. 1. a) Detail of the plates manufactured, the positioning of the specimens in the plate and b) detail of the specimens tested. All dimensions are in mm and dimensions are not to scale.
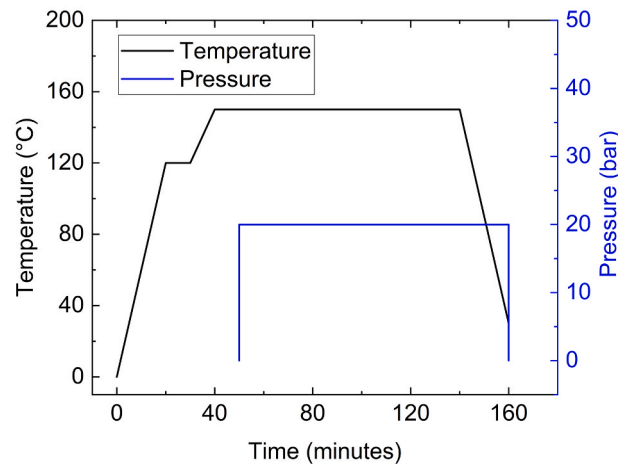

Fig. 2. Temperature and pressure variation during the cure cycle for the TBDC panels.

through the thickness and the lack of resin rich areas due to the optimised manufacturing process.

2.2. Fatigue testing protocol

The fatigue testing was carried out based on the ASTM D3479 [25] standard for tension-tension loading. The dimensions of the specimens were 150 × 15 mm, and aluminium tabs were used covering 50 mm from each end of the specimen, leaving a gauge length of 50 mm (see Fig. 1b). The testing was conducted on a universal loading machine with a load cell of 100 kN. The cyclic tension-tension loading was controlled using a sinusoidal wave shape with the R value (ratio between the minimum and maximum stress) being 0.1. A frequency of 5 Hz was utilised to avoid overheating of the specimens following relevant studies [24]; sporadic measurements during testing validated that the specimens were indeed not overheating. Fig. 4 shows the experimental setup and a sketch of the sinusoidal wave shape applied to the specimens.

The load/displacement curves were recorded while testing. The load was converted to stress using the specimens' cross-section dimensions, while the stress was divided by the longitudinal stiffness of the specimens to extract the maximum cyclic strain. The longitudinal stiffness of the specimens was determined from quasi-static testing on the same
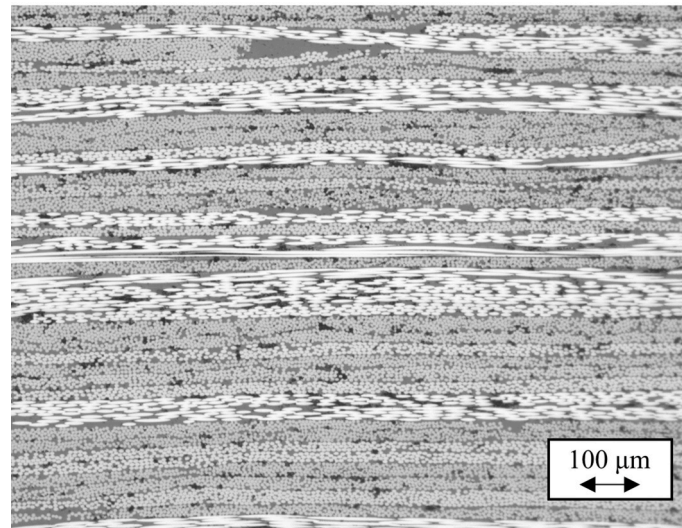
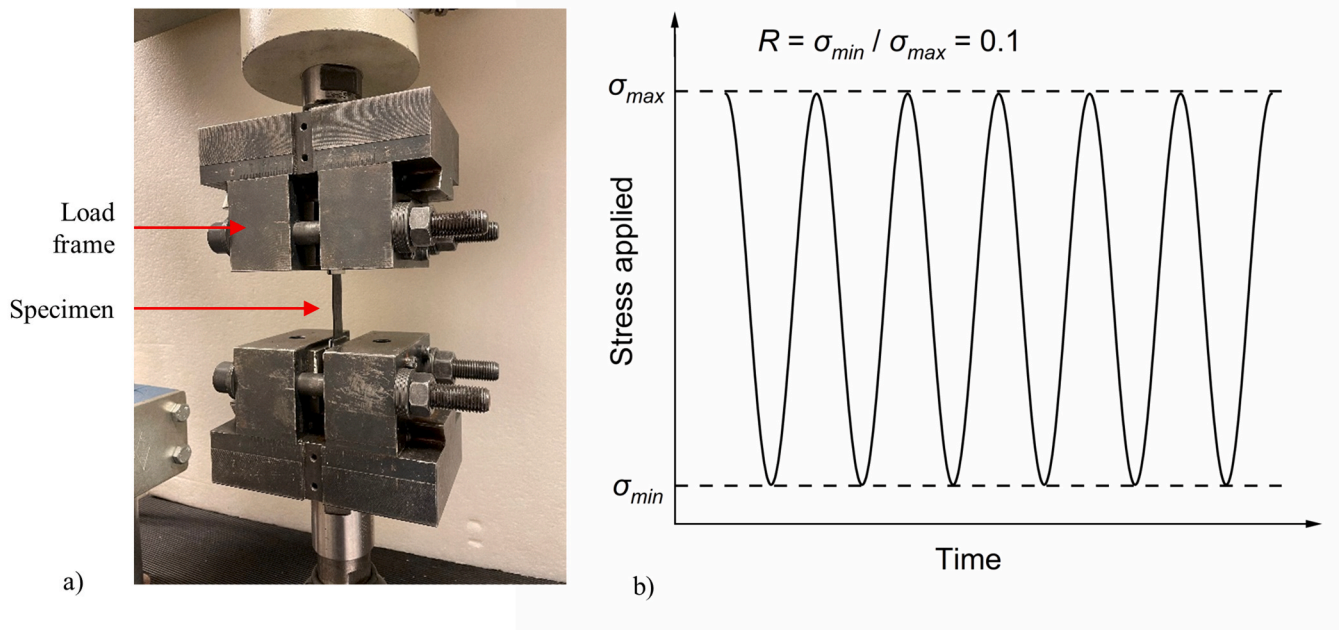**Fig. 3.** Characteristic cross section of the TBDC specimens.

Fig. 4. a) Experimental setup for the fatigue testing campaign and b) sketch of the sinusoidal wave shape loading applied to the specimen.

specimens; details of the quasi-static testing and relevant measurements can be found in Ref. [5]. Following that, *S–N* (maximum stress vs cycles to failure) curves were generated. The testing was stopped for specimens which lasted over 2×10^6 cycles and these specimens were annotated as run-out specimens. The results were also expressed as a percentage in relation to the static strength, to allow for easier comparisons with other studies on similar materials. Finally, the results were also normalised in relation to their density to allow for comparisons with more conventional materials such as steel, titanium, and aluminium.

2.3. SEM analysis

SEM was used to examine the fracture surfaces of the specimens after fatigue loading. It was attempted to study characteristic specimens subjected to low and high cycle fatigue to identify differences in the damage mechanisms. Characteristic fracture surfaces were identified, cut to size, and were mounted on stubs for analysis. A thin layer of gold sputter was applied on the surfaces and a JEOL 7800 F prime was used for the analysis. Magnification levels between x100 and x8000 were considered while the acceleration voltage was varied between 2 and 5 kV.

2.4. Fibre volume fraction

The fibre volume fraction of the specimens was measured using the matrix digestion in nitric acid method following ASTM D3171. Characteristic specimens from different parts of the plate were selected, and their mass was measured before and after the acid digestion (m_c and m_f respectively). The dimensions of the specimens tested were about 15×30 mm. The density of the fibres and the resin was provided by the

manufacturer (ρ_f and ρ_m respectively) and the fibre volume fraction was calculated following equation (1).

$$V_f = \frac{1}{1 + \frac{\rho_f}{\rho_m}\left(\frac{m_c}{m_f} - 1\right)} \tag{1}$$

3. Results

3.1. S–N curves

Fig. 5 shows the *S–N* curves obtained in a semi-log plot for specimens cut along the horizontal (x) and vertical (y) direction of the TBDC panel. Trendlines were added in the plots using a linear fit function and they display similar slopes for both directions. The average static strength values measured from this plate were also included in the plot but were not taken into consideration for the calculation of the trendlines. In addition, for comparison purposes, the static strength values obtained in Ref. [5] were also included in the plot. Most of the data points are concentrated between 10^3 and 10^6 cycles while there were also three run-out specimens for the x direction, and two run-out specimens for the y direction. It is worth noting that the specimens which failed in the end tab zones were excluded from the analysis and thus a total of 20 specimens were considered.

The static, in-plane isotropic properties for the thin TBDC specimens were validated in a previous publication by the authors by showing minimal differences between the static strength and stiffness in the x and y orientations [5]. Fig. 5 shows that the in-plane isotropic response of the TBDC materials expanded to their fatigue performance. More specifically, the fatigue measurements were not influenced by the direction of the specimens. The difference in the slopes of the trendlines shown in Fig. 5 is minimal and can be explained by microstructural variability, including fibre volume fraction, tape orientation, location of tow ends, and edge effects. In this context, edge effects refer to the positioning of certain specimens near the edges of the panel where the variation is expected to be higher. The fibre volume fraction of three specimens was measured from random parts of the plate and the average value was determined as 63.9 ± 6.1 %. The scatter in the fibre volume fraction measurements can justify the experimental scatter in the fatigue testing.

3.2. Damage mechanisms

3.2.1. Macroscopic damage

Fig. 6 shows typical fracture surfaces from selected tested specimens subjected to static loading, low and high cycle fatigue. It is noted that after failure, two fracture surfaces are generated for each specimen. Fig. 6a, c and 6e show both fracture surfaces for the static, low cycle fatigue specimen and high cycle fatigue specimen respectively. Fig. 6b, d and 6f show a higher magnification on the same fracture surfaces in the location indicated by the red boxes. On the macroscopic scale, a combination of damage mechanisms, including fibre fracture and tape pull-out can be observed for both specimens. The main differentiation between the static, low and high cycle fatigue specimens is related to the size of the damaged area. The static and low cycle fatigue failure produced generally smaller fracture surfaces and more clearly defined failure planes as shown in Fig. 6a–d. In contrast, the high cycle fatigue failure was characterised by large surface fractures as shown in Fig. 6e and f. The length of the pulled-out features on the fracture surfaces can be seen by following the yellow lines marked on the figures.

3.2.2. SEM analysis

Fig. 7 shows characteristic damage features in the TBDC specimens after static and fatigue loading. As discussed in Ref. [5], after static loading, shear mode II cusps are developed during the matrix deformation which lead to tape pull-out. The shear cusps after static testing are elevated as shown in Fig. 7a. Similar observations were also made for the fatigue loading case shown in Fig. 7b. Extensive matrix deformation was observed, and shear cusps were generated. However, this time the cusps were not elevated but they were deteriorated instead, resembling matrix rollers in appearance. Shear cusps in the form of matrix rollers have been identified in the past by other authors during fatigue shear loading [26,27], thereby validating these findings.

Fig. 8 shows two characteristic cases of specimens that failed after low and high cycle fatigue. The low cycle fatigue specimen failed at 12801 cycles with a maximum applied stress of 490 MPa, while the high cycle fatigue specimen failed at 308332 cycles with a maximum applied stress of 420 MPa. The main difference that can be observed between the fracture surfaces of the failed specimens is the size and shape of the shear cusps which deteriorated into matrix rollers. More specifically, Fig. 8a shows the low cycle fatigue case, where there is evidence of the transformation of the elevated shear cusps into matrix rollers, which are fully developed and can be identified more clearly in Fig. 8b for the high cycle fatigue case.
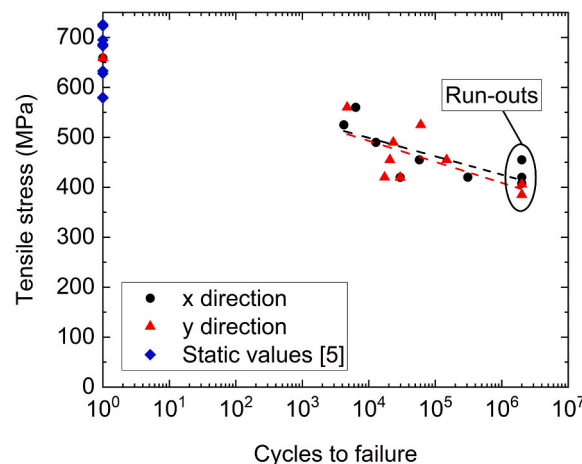

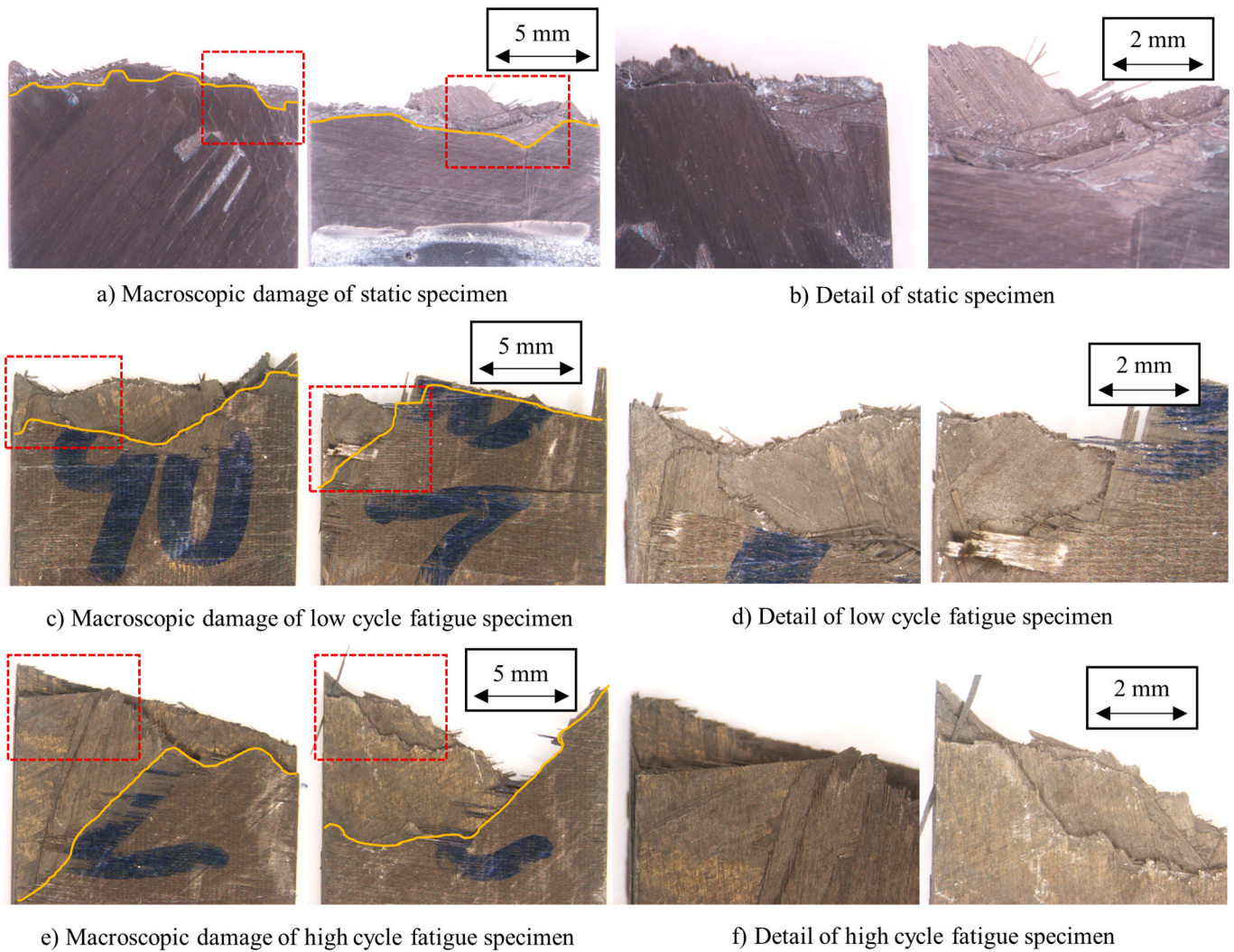**Fig. 5.** S–N curves for the different x and y orientations.

a) Macroscopic damage of static specimen

b) Detail of static specimen

c) Macroscopic damage of low cycle fatigue specimen

d) Detail of low cycle fatigue specimen

e) Macroscopic damage of high cycle fatigue specimen

f) Detail of high cycle fatigue specimen

Fig. 6. Fracture surfaces after static (a and b), low cycle (c and d), and high cycle (e and f) fatigue.

4. Discussion

4.1. Comparison with the literature for QI and TBDC laminates

As presented in section 3, the run-out specimens were tested under a maximum cyclic stress of at least 380 MPa and a maximum cyclic strain above 0.5 %. These values can be considered as the fatigue limit of the TBDC material. This response is considered high-performance especially in the context of quasi-isotropic composites and similar TBDC materials. Fig. 9a compares the fatigue response (in terms of *S–N* curves) of the TBDC materials studied in this paper with other similar TBDC materials [23,24] and QI [0, 45,-45,90]$_s$ continuous-fibre CFRP laminates [28]. Fig. 9b shows the same comparison after normalising the applied stress by the static strength (UTS) of each material. It is worth noting that Fig. 9b includes two additional studies [21,29] which reported only normalised data. Fig. 9 shows only the trendlines (and not the data points) to enhance readability. For this work's S–N curve, the y-direction data points were plotted in these comparisons since they resulted in the lowest static strength and fatigue limit and thus were considered more conservative.

The fatigue resistance of the TBDC material studied here is significantly higher in terms of applied stress, compared to other high performing TBDCs and QI laminates. More specifically, the fatigue strength of the TBDC material reported in this study drops from 500 MPa to 400 MPa for a cycle range between 10^3 and 10^6, while the TBDC responses

reported by other authors [23,24] did not exceed 200 MPa for the same number of cycles; the most likely explanation for this difference is the tow/tape thickness: this work used 21 μm thick tapes, while the other studies [23,24,29] used 100–150 μm thick tapes. The fatigue resistance of the QI laminate was in the range of 200–300 MPa for the same number of cycles. It is worth noting however, that the QI laminate reported in Ref. [28] was made out of thick plies (around 200 μm) which justifies the relatively low fatigue values reported.

Due to the significant differences in the tensile strength and fatigue resistance, the applied stress was normalised against the ultimate tensile stress of each material. After normalising the data, the results between the different studies converged more. The results reported by Martulli et al. [24] showed a slightly flatter slope and thus smaller sensitivity to fatigue loading while retaining a higher percentage of their static strength. The rest of the studies displayed steeper slopes and/or lower fatigue resistance. Overall, the slope differences between the trendlines of different studies were small. This can be justified by the fact that the literature review focused only on CFRP materials (TBDC and QI) which are expected to have similar sensitivity to fatigue loading.

For the static tests, it was shown [5] that the static strength was at least 30 % higher compared to any other TBDC/SMC material reported in the literature. A similar trend is now demonstrated for the fatigue response, as the fatigue limit is significantly higher compared to other similar materials. The improved performance is a result of the micro-architecture of the ultra-thin TBDC which combines stiff and
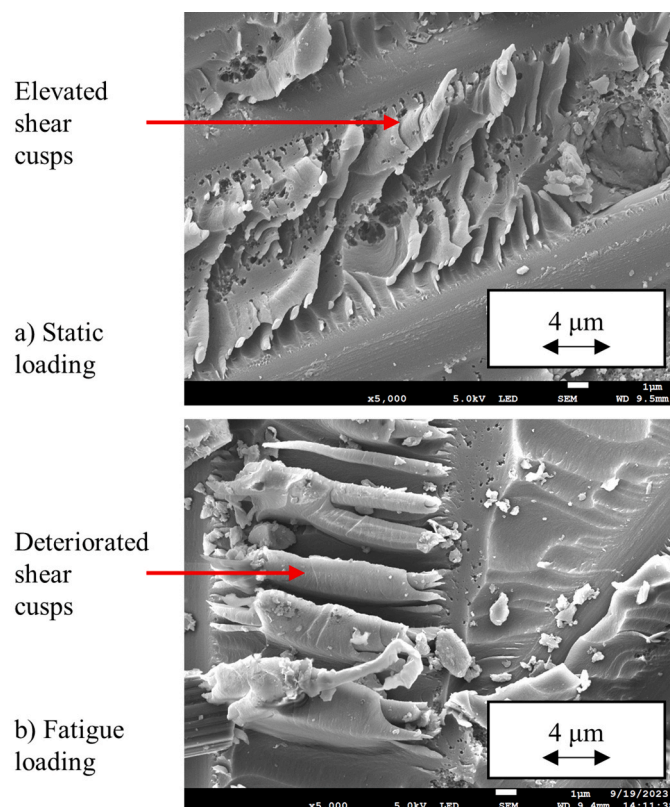
Fig. 7. SEM analysis of the fracture surfaces of a) static and b) fatigue tested TBDC specimens (magnification level x5000).
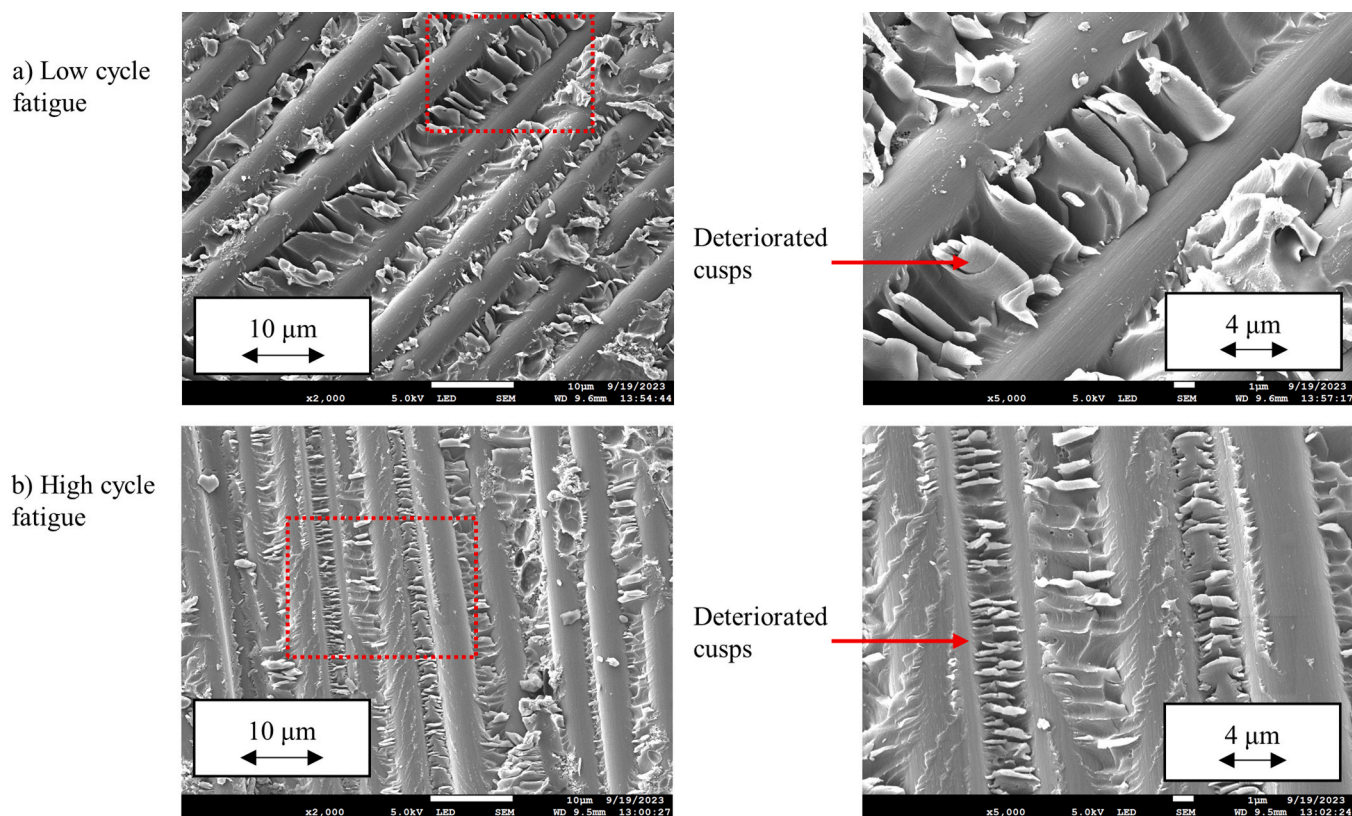

Fig. 8. Comparison of the fracture surfaces of a) low and b) high cycle fatigue damage characteristics.
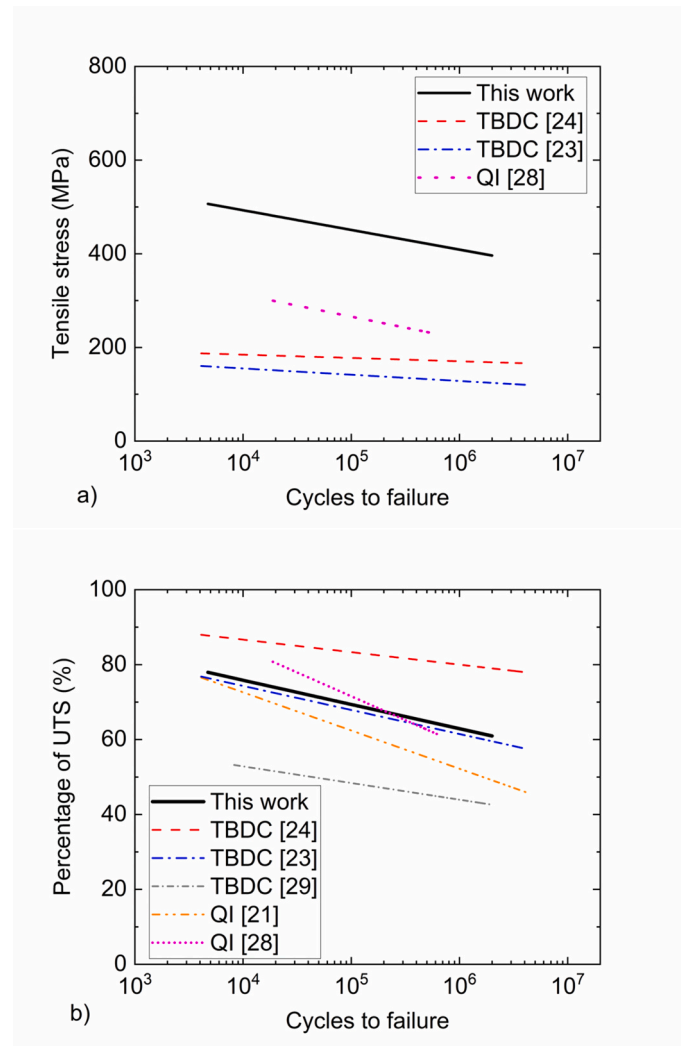
Fig. 9. Comparison of the fatigue resistance of the TBDC material with other SMCs and QI continuous-fibre laminates based on a) absolute stress values and b) normalised stress values as a percentage of their UTS. In all reported studies, R = 0.1 (except the QI in Ref. [21] where R = 0).
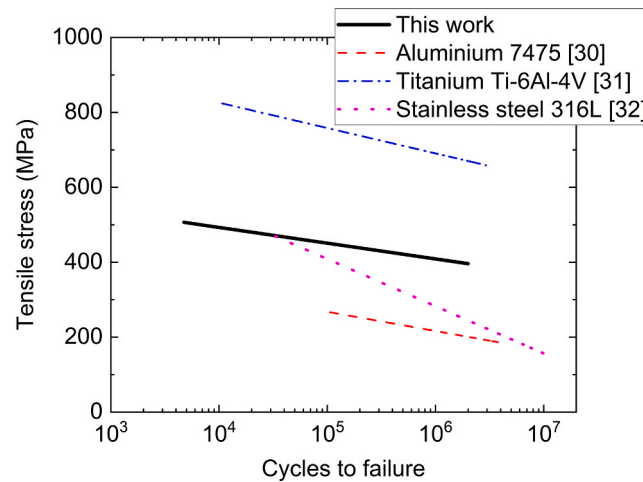

Fig. 10. Comparison of the fatigue resistance of the TBDC material with conventional metals based on absolute stress values.

ultra-thin tapes. In addition, the optimised manufacturing methods, combining pre-impregnated tapes with high moulding pressures, result in higher fibre volume fractions and increased strength.

4.2. Comparison with the literature for metals

The main advantage of composite materials compared to their metallic counterparts is related to their high specific strength which is a result of their low density. The density of conventional structural metals can be up to 5 times higher compared to CFRP composites. Therefore, one additional comparison is presented here where the TBDC material fatigue response is compared with literature values for typical alloys of aluminium, titanium, and stainless steel [30–32]. Fig. 10 compares the fatigue response of the TBDC material with three metals in terms of *S–N* curves.

Fig. 10 shows that the TBDC material studied here has higher fatigue resistance compared to aluminium and stainless steel with a fatigue limit about two times higher in terms of stress. Titanium, however, reached significantly higher stress levels and displayed a fatigue limit of about 700 MPa. These results showcase the ability of the TBDC material to be compared directly with metals. However, it was also considered appropriate to normalise these results with the density of each material, as this would provide a more accurate indication of their performance. Therefore, Fig. 11 presents the same *S–N* curves after normalising the y axis with the density of each material (i.e. the specific S–N curves). The density values assumed were 7.85 g cm^{-3} for the stainless steel, 4.50 g cm^{-3} for the titanium, 2.50 g cm^{-3} for the aluminium and 1.60 g cm^{-3} for the TBDC material. The units of the normalised stress were expressed in kN m kg^{-1}.

Fig. 11 highlights the effect of density. More specifically, the TBDC material displayed the best specific fatigue response with a specific fatigue limit about 1.5 times higher compared to the titanium, 3 times higher compared to aluminium and almost 9 times higher compared to stainless steel. These results show the versatility and excellent mechanical properties of the thin-tape TBDC materials, while also highlighting the importance of taking the density into consideration in the selection of materials during design of structures for fatigue loading.

5. Conclusions

This present study focuses on the fatigue response of Tow-Based Discontinuous Composites with thin-tapes by employing an experimental campaign including mechanical testing and optical and scanning electron microscopy. A critical interpretation of the results was also presented by comparing the fatigue performance with other TBDCs and QI laminates along with more conventional metals. The main conclusions of the study are summarised as follows.

- The fatigue response of the ultra-thin TBDC specimens was demonstrated as high-performance since the specimens reached a fatigue limit of at least 380 MPa and 0.5 % strain. The in-plane isotropic performance was validated for cyclic loading as specimens in both directions of the panels were tested and produced similar results.
- The experimental scatter in the fatigue testing was justified by microstructural variability, including fibre volume fraction, tape orientation, location of tow ends, and edge effects.
- The optical microscopy revealed differences in the fracture surfaces of static, low, and high-cycle fatigue specimens. More specifically, the static and low-cycle fatigue specimens produced generally smaller pull-out features in the fracture surfaces and more clearly defined failure planes. In contrast, the high-cycle fatigue failure was characterised by large surface fractures.
- The SEM analysis also revealed significant differences between the static failure, the low-cycle fatigue, and the high-cycle fatigue. The differences were mostly related to the matrix deformation. In the static case, shear cusps which are related to shear fracture and tape pull-out were identified. In the case of fatigue fracture surfaces, the shear cusps were still present, but their size and shape were different. More specifically, for the low-cycle fatigue, the shear cusps were slightly deteriorated and started forming matrix rollers, while for the high-cycle fatigue, the shear cusps were completely deteriorated, and the matrix rollers were fully developed.
- A critical comparison with other standard-thickness TBDCs and QI carbon fibre laminates highlighted the outstanding properties of the ultra-thin TBDC materials as they displayed significantly higher fatigue strength limits. Similarly, such comparisons were also performed between the ultra-thin TBDC materials and conventional metals, and it was shown that the TBDCs have higher fatigue resistance compared to stainless and steel and aluminium and lower fatigue resistance compared to titanium. Moreover, when the results were normalised based on the material density, the ultra-thin TBDCs clearly outperformed all their metal counterparts highlighting their suitability for high-end engineering applications.
- The results highlight the beneficial effects of the optimised manufacturing methods (using pre-impregnated tapes with high moulding pressures) on the performance of randomly oriented discontinuous composites and demonstrate the potential of these materials to be used in demanding structural applications. Therefore,
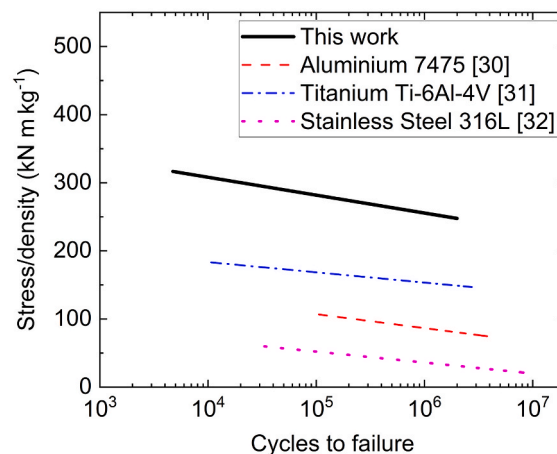

Fig. 11. Comparison of the fatigue resistance of the TBDC material with conventional metals based on density normalised stress values.

the novelty of the study is evident, showing new application potentials for an innovative material concept.

CRediT authorship contribution statement

Ioannis Katsivalis: Writing – original draft, Software, Methodology, Investigation, Formal analysis, Data curation, Conceptualization. **Monica Norrby:** Writing – review & editing, Investigation. **Florence Moreau:** Writing – review & editing, Resources. **Erik Kullgren:** Writing – review & editing, Resources. **Soraia Pimenta:** Writing – review & editing, Methodology, Investigation, Funding acquisition, Formal analysis, Conceptualization. **Dan Zenkert:** Writing – review & editing, Methodology, Investigation, Funding acquisition, Formal analysis, Conceptualization. **Leif E. Asp:** Writing – review & editing, Methodology, Investigation, Funding acquisition, Formal analysis, Conceptualization.

Declaration of competing interest

The authors declare that they have no known competing financial interests or personal relationships that could have appeared to influence the work reported in this paper.

Data availability

Data will be made available on request.

Acknowledgements

References

[1] Kupski J, Teixeira de Freitas S, Zarouchas D, Camanho PP, Benedictus R. Composite layup effect on the failure mechanism of single lap bonded joints. Compos Struct 2019;217:14–26.

[2] Katsivalis I, Signorini V, Ohlsson F, Langhammer C, Minelli M, Asp LE. Hydrogen permeability of thin-ply composites after mechanical loading. Compos Appl Sci Manuf 2024;176:107867.

[3] Li Y, Pimenta S, Singgih J, Nothdurfter S, Schuffenhauer K. Experimental investigation of randomly-oriented tow-based discontinuous composites and their equivalent laminates. Compos Appl Sci Manuf 2017;102:64–75.

[4] Alves M, Carlstedt D, Ohlsson F, Asp LE, Pimenta S. Ultra-strong and stiff randomly-oriented discontinuous composites: Closing the gap to quasi-isotropic continuous-fibre laminates. Compos Appl Sci Manuf 2020;132.

[5] Katsivalis I, Persson M, Johansen M, Moreau F, Kullgren E, Norrby M, Zenkert D, Pimenta S, Asp LE. Strength analysis and failure prediction of thin tow-based discontinuous composites. Compos Sci Technol 2024;245:110342.

[6] Camanho PP, Dávila CG, Pinho ST, Iannucci L, Robinson P. Prediction of in situ strengths and matrix cracking in composites under transverse tension and in-plane shear. Compos Appl Sci Manuf 2006;37:165–76.

[7] Wan Y, Takahashi J. Development of carbon fiber-reinforced thermoplastics for mass-produced automotive applications in Japan. J. Composites Sci. 2021:86.

[8] Yamashita S, Sonehara T, Takahashi J, Kawabe K, Murakami T. Effect of thin-ply on damage behaviour of continuous and discontinuous carbon fibre reinforced thermoplastics subjected to simulated lightning strike. Compos Appl Sci Manuf 2017;95:132–40.

[9] Alves M, Li Y, Pimenta S. Spatial variability and characteristic length-scales of strain fields in tow-based discontinuous composites: characterisation and modelling. Compos B Eng 2023;262:110789.

[10] Alves M, Pimenta S. The influence of 3D microstructural features on the elastic behaviour of tow-based discontinuous composites. Compos Struct 2020;251.

[11] Gulfo L, Haglund Nilsson O, Sjöberg J, Katsivalis I, Asp LE, Fagerström M. A 3D voxel-based mesostructure generator for finite element modelling of tow-based discontinuous composites. Compos B Eng 2024;278:111405.

[12] Hiley M. 5 - fatigue failures of polymer composites. In: Greenhalgh ES, editor. Failure analysis and Fractography of polymer composites. Woodhead Publishing; 2009. p. 238–78.

[13] Guo R, Li C, Niu Y, Xian G. The fatigue performances of carbon fiber reinforced polymer composites – a review. J Mater Res Technol 2022;21:4773–89.

[14] Alam P, Mamalis D, Robert C, Floreani C, Ó Brádaigh CM. The fatigue of carbon fibre reinforced plastics - a review. Compos B Eng 2019;166:555–79.

[15] Brunbauer J, Pinter G. Effects of mean stress and fibre volume content on the fatigue-induced damage mechanisms in CFRP. Int J Fatig 2015;75:28–38.

[16] Talreja R. Fatigue of composite materials: damage mechanisms and fatigue-life diagrams. Proc. Royal Soc. London. A. Mathemat. Phys. Sci. 1981;A378:461–75.

[17] Kawai M. 12 - fatigue life prediction of composite materials under constant amplitude loading. In: Vassilopoulos AP, editor. Fatigue life prediction of composites and composite structures. second ed. Woodhead Publishing; 2020. p. 425–63.

[18] Tang H, Zhou G, Chen Z, Huang L, Avery K, Li Y, Liu H, Guo H, Kang H, Zeng D, Engler-Pinto C, Su X. Fatigue behavior analysis and multi-scale modelling of chopped carbon fiber chip-reinforced composites under tension-tension loading condition. Compos Struct 2019;215:85–97.

[19] Bartkowiak M, Kizak M, Liebig WV, Weidenmann KA. Fatigue behavior of hybrid continuous-discontinuous fiber-reinforced sheet molding compound composites under application-related loading conditions. Composites Part C: Open Access 2022;8:100265.

[20] Gamstedt EK, Talreja R. Fatigue damage mechanisms in unidirectional carbon-fibre-reinforced plastics. J Mater Sci 1999;34:2535–46.

[21] Selezneva M, Lessard L. Characterization of mechanical properties of randomly oriented strand thermoplastic composites. J Compos Mater 2015;50:2833–51.

[22] Martulli LM, Muyshondt L, Kerschbaum M, Pimenta S, Lomov SV, Swolfs Y. Carbon fibre sheet moulding compounds with high in-mould flow: linking morphology to tensile and compressive properties. Compos Appl Sci Manuf 2019;126:105600.

[23] Tang H, Chen Z, Zhou G, Sun X, Li Y, Huang L, Guo H, Kang H, Zeng D, Engler-Pinto C, Su X. Effect of fiber orientation distribution on constant fatigue life diagram of chopped carbon fiber chip-reinforced Sheet Molding Compound (SMC) composite. Int J Fatig 2019;125:394–405.

[24] Martulli LM, Muyshondt L, Kerschbaum M, Pimenta S, Lomov SV, Swolfs Y. Morphology-induced fatigue crack arresting in carbon fibre sheet moulding compounds. Int J Fatig 2020;134:105510.

[25] ASTM. D3479/D3479M-19(2023), standard test method for tension-tension fatigue of polymer matrix composite materials. West Conshohocken, PA: ASTM International; 2023.

[26] Hiley MJ. Fractographic study of static and fatigue failures in polymer composites. Plast, Rubber Compos 1999;28:210–27.

[27] Sjögren A, Asp LE. Effects of temperature on delamination growth in a carbon/epoxy composite under fatigue loading. Int J Fatig 2002;24:179–84.

[28] Aithal S, Padmaraj NH, Kini MV, Pai D. Fatigue durability test of quasi-isotropic carbon/epoxy laminates in marine environment. Adv Manuf Polym Compos Sci 2023;9:2275097.

[29] Sieberer S, Nonn S, Schagerl M. Fatigue behaviour of discontinuous carbon-fibre reinforced specimens and structural parts. Int J Fatig 2020;131:105289.

[30] Verma BB, Atkinson JD, Kumar M. Study of fatigue behaviour of 7475 aluminium alloy. Bull Mater Sci 2001;24:231–6.

[31] Li P, Warner DH, Fatemi A, Phan N. Critical assessment of the fatigue performance of additively manufactured Ti–6Al–4V and perspective for future research. Int J Fatig 2016;85:130–43.

[32] Zeng F, Yang Y, Qian G. Fatigue properties and S-N curve estimating of 316L stainless steel prepared by SLM. Int J Fatig 2022;162:106946.